Photochemistry and Photobiology, 1998, 67(1): 41–49

Symposium-in-Print

Ultrasonic Modulation of Scattered Light in Turbid Media and a Potential Novel Tomography in Biomedicine

Lihong V. Wang*

Optical Imaging Laboratory, Biomedical Engineering Program, Texas A&M University, College Station, TX

Received 15 April 1997; accepted 2 October 1997

ABSTRACT

Ultrasonic modulation of scattered laser light was used to image objects buried in tissue-simulating turbid media. The ultrasonic wave focused into the turbid media modulated the laser light passing through the ultrasonic field. The modulated laser light collected by a photomultiplier tube reflected primarily the local mechanical and optical properties in the zone of ultrasonic modulation. A raster scanning over a heterogeneous turbid medium yielded an image of the medium based on the ultrasound-modulated optical signal. The detectability of modulated signal was estimated using diffusion theory. The dependence of the modulated signal on the off-axis distance of the detector from the optic axis and on the amplitude of ultrasound was studied. The mechanisms of ultrasonic modulation of scattered light are discussed. A theory based on the field autocorrelation function is reviewed as well.

INTRODUCTION

Nonoptical imaging

Medical imaging has been one of the most exciting areas for engineering application in medicine in this century. Although medical imaging has many diagnostic applications, breast cancer detection will be used as an example in this paper to illustrate the significance of optical imaging. Breast cancer is the most common malignant neoplasm and the leading cause of cancer deaths in women in the United States. A means for prevention of breast cancer has not been found, and early detection and treatment are the best way to improve cure rate. At present, mammography and ultrasonography are clinically used for breast cancer detection. Mammography is currently the only reliable means of detecting nonpalpable breast cancers. As a supplementary tool, ultrasound is used to evaluate the internal matrices of circumscribed masses found at mammography or of palpable masses that are obscured by radiographically dense parenchyma at mammography (1–3). However, X-ray mammography consists of ionizing radiation, and imaging of radiographically dense breasts is difficult. Ultrasonography cannot detect many of the nonpalpable cancers that are not visible on mammograms of good quality (2). Most of the studies claiming that ultrasonography is useful in this regard compare it to poor-quality mammography or fail to compare it to mammography.

Several other techniques are under investigation for breast cancer imaging. Magnetic resonance imaging (MRI)† offers great promise for imaging of the radiographically dense breast (4,5). Breast MRI is superior to mammography in differentiating solid from cystic lesions and is equivalent to mammography in providing information regarding different parenchymal patterns. Injection of intravenous contrast material with MRI increases cancer detectability in spite of the fact that breast cancer and glandular tissues have similar magnetic resonance tissue characteristics. However, breast MRI is expensive, has inferior spatial resolution to mammography, and cannot image microcalcifications (2,6).

The ability of Breast computed tomography (CT) to differentiate benign from malignant solid masses has been investigated. Breast CT involves the use of intravenous injection of iodinated contrast material and has limited spatial resolution and high cost; hence, it is not suited for routine breast cancer screening (2).

Optical imaging

Nonionizing laser light imaging of breast cancer is a new and active research field although incoherent light imaging was investigated as early as 1929 (7,8). The optical properties (see Appendix) of normal and diseased breast tissues are usually different despite the large variation of values in optical properties (9–11). Therefore, it is possible to detect some breast cancers based on measurements of optical properties.

The optical difference is not surprising because cancerous tissues manifest significant architectural changes at the cel-

*To whom correspondence should be addressed at: Biomedical Engineering Program, Texas A&M University, College Station, TX 77843-3120, USA. Fax: 409-847-9005; e-mail: lwang@tamu.edu

†*Abbreviations:* CT, computed tomography; mfp, mean free path; MRI, magnetic resonance imaging; NIR, near-infrared; PMT, photomultiplier tube.

lular and subcellular levels, and the cellular components that cause elastic scattering have dimensions typically on the order of visible to near-infrared (NIR) wavelengths. Some tumors are associated with vascularization, where blood causes increased light absorption. Optical contrast agents may also be exploited to enhance the optical contrast between normal and abnormal tissues (12). Because the optical information is determined by the molecular conformations of biological tissues, optical imaging is expected to provide sensitive signatures for early breast cancer detection and monitoring.

Because tissues are optically turbid media that are highly scattering, light is quickly diffused inside tissues as a result of frequent scattering. A typical scattering coefficient for visible light in biological tissues is 100 cm^{-1}, compared to 0.2 cm^{-1} for X-ray used in medical diagnostics. Light transmitted through tissues is classified into three categories: ballistic light, quasi-ballistic light and diffuse light. Ballistic light experiences no scattering by tissue and thus travels straight through the tissue. Ballistic light carries direct imaging information as X-ray does. Quasi-ballistic light experiences minimal scattering and carries some imaging information. Multiply scattered diffuse light carries little direct imaging information and overshadows ballistic or quasi-ballistic light.

One of the techniques is called "early-photon imaging" (13). If diffuse light is rejected and ballistic or quasi-ballistic light is collected, buried objects can be detected. This technique uses a short-pulse laser (<1 ps pulse width) to illuminate the breast tissue. Only the initial portion of transmitted light is allowed to pass to a light detector, and the late-arriving light is gated off by a fast optical gate. If only ballistic light is detected the technique is called ballistic imaging. It has been shown that ballistic imaging is feasible only for breast tissue of thickness less than 1.4 mm or 42 mean free paths (mfp) (14,15). Most ballistic imaging techniques reported in the literature have achieved approximately 30 mfp. Therefore, this approach is suitable for thin tissue samples but suffers loss of signal and resolution for thick tissues as a result of strong scattering of light by the tissue.

For breast tissue of clinically useful thickness (5–10 cm), scattered light must be used to image breast cancers. We have shown that for a 5 cm thick breast tissue with the assumed absorption coefficient $\mu_a = 0.1\ cm^{-1}$ and reduced scattering coefficient $\mu_s' = 10\ cm^{-1}$, the detector must collect transmitted light that has experienced at least 1100 scattering events in the tissue to yield enough signal (15). Therefore, ballistic light or even quasi-ballistic light does not exist for practical purposes. However, if a 10 mW visible or NIR laser is incident on one side of the 5 cm thick breast tissue, we have estimated using diffusion theory that the diffuse transmittance is on the order of 10 nW/cm^2 or 10^{10} photons/$(s \cdot cm^2)$, which is detectable using a photomultiplier tube capable of single-photon counting. Similarly, the diffuse transmittance through a 10 cm thick breast tissue would be on the order of 1 pW/cm^2 or 10^6 photons/$(s \cdot cm^2)$. The significant transmission of light is a result of the low absorption coefficient despite the high scattering coefficient.

Resolution of pure laser imaging degrades linearly with increased tissue thickness (16). Hebden *et al.* (17) detected the temporal profiles of the scattered light using a streak camera and then mathematically extrapolated the signal to the early part of the profiles in which the actual light could not be detected. The early portion of the profiles was integrated to construct the images of buried objects (8 mm diameter) in a turbid medium (51 mm thick). The spatial resolution was found to be 5 mm for a 5 cm thick breast phantom (18), which agreed with the theoretical prediction (16). This time domain technique requires expensive short-pulse lasers and fast light detectors.

Another technique for laser light imaging is the frequency domain technique, also called photon density wave imaging, which was first introduced into the field by Fishkin and Gratton (19). This technique uses amplitude-modulated laser light (at approximately 100 MHz) to illuminate the tissue and detects the diffuse light. The imaging resolution of this technique is similar to that of the time domain technique but usually requires complex imaging reconstruction algorithms.

Marks *et al.* (20) investigated tissue imaging using the combination of pulsed ultrasound and laser light. They detected the ultrasound-modulated optical signal in a homogeneous turbid medium without buried objects. Wang *et al.* (21,22) imaged buried objects in tissue-simulating turbid media using continuous-wave ultrasound-modulated optical tomography. The major advantage of continuous-wave ultrasonic modulation over pulsed ultrasonic modulation was the significant increase in signal-to-noise ratio, which allowed one to image buried objects in turbid media. Leutz and Maret (23) reported the observation and theoretical analysis of ultrasonic modulation of multiple-scattering speckles. Kempe *et al.* (24) investigated the modulation of the optical field transmitted through a turbid medium by a quasi-continuous-wave ultrasound beam.

Ultrasound-modulated optical tomography measures the mechanical and optical properties of tissues, whereas X-ray mammography measures radiographical density of tissues and ultrasonography measures echogenicity of tissues. Ultrasound-modulated optical tomography is free of the hazards of ionizing radiation associated with mammography and separates the resolution and signal problem of light-only imaging because the resolution is determined by the size of the ultrasound focus and the signal depends on any light passing through the ultrasound focal zone including ballistic, quasi-ballistic and diffuse light.

This paper reviews the state of the art in ultrasonic modulation of scattered light and ultrasound-modulated optical tomography. The theoretical aspects reported in this paper include the physical mechanisms of ultrasonic modulation of scattered light in turbid media, modeling of the modulation and expected signal strength of the modulated signal in biological tissues. The experimental aspects include the observation of the modulated signal, its dependence on different parameters and tomography of objects buried in turbid media.

MECHANISMS OF ULTRASONIC MODULATION

A typical configuration of acousto-optical experiments in turbid media is shown in Fig. 1. Laser light is incident upon the turbid medium. An ultrasonic wave that may or may not be focused propagates into a turbid medium. The ultrasonic wave modulates light passing through the ultrasonic field. A

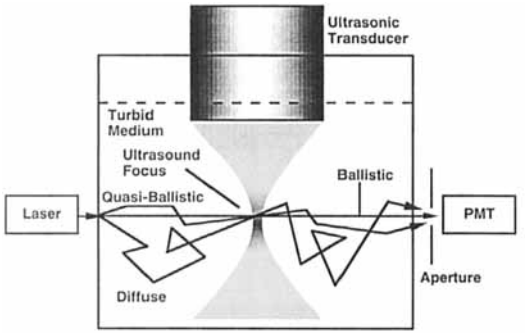

Figure 1. Illustration of the hypothesis of ultrasound-modulated optical tomography.

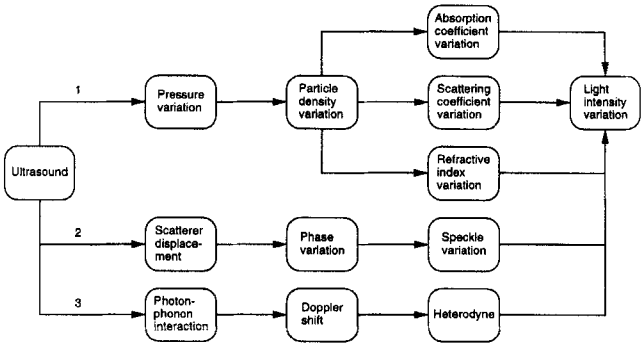

Figure 2. List of possible mechanisms of ultrasonic modulation of light in turbid media.

photodetector such as a photomultiplier tube (PMT) converts optical signal into electronic signal for detection. The ultrasound-modulated signal may be separated from the unmodulated signal.

Discussion of several possible modulation mechanisms follows (Fig. 2). Approach 1 is caused by pressure variation in response to the ultrasonic wave. The pressure variation induces a density change in the medium as a result of the compressibility of the medium. The optical absorption and scattering coefficients are proportional to the number density of absorbers and scatterers, respectively. The index of refraction varies with the density as well. Therefore, the density variation modulates the optical properties of the medium at the ultrasonic frequency. The variation of optical properties modulates the intensity of the light passing through the ultrasonic field. Approach 1 does not require coherence for the light source.

Approach 2 is caused by scatterer displacement in response to the ultrasonic wave. The scatterer displacement causes the optical path length of scattered photons to change. Coherent laser light passing through turbid media generates speckles. Because speckles depend on the optical path length, the speckles vary due to the ultrasonic modulation of scatterer displacements.

Approach 3 is caused by photon-phonon interactions. An ultrasonic wave may be considered as phonons and light may also be considered as photons. The photon–phonon interactions cause Doppler shift (25) in the classical sense to the frequency of the photons by the ultrasonic frequency and its harmonics. An optical detector functions as a heterodyning device between the Doppler-shifted light and unshifted light and produces an intensity signal at the ultrasonic frequency and its harmonics. This mechanism is similar to Brillouin scattering, where the phonons are of thermal origin (25).

Approaches 2 and 3 require coherence for the light source and both may be considered speckle effect. The modulation of the speckles in approach 2 is caused by the ultrasonic modulation of scatterer displacements, while the modulation of the speckles in approach 3 is caused by the ultrasonic modulation of refractive index of the medium. The two types of modulation are separated in this paper for clarity.

The ultrasonic modulation of refractive index appears in both approaches 1 and 3. In approach 1, the variation of refractive index causes light that may or may not be coherent to fluctuate in intensity. In approach 3, the variation of refractive index causes fluctuation in phase of coherent light, which is converted to fluctuation in intensity by a square-law detector.

We replaced the laser with a white light source in the ultrasound-modulated optical tomography setup but observed no ultrasound-modulated optical signal (26), which was confirmed more recently using a super-luminescent diode that emitted light of short coherence length. This result showed that approach 1 can be ruled out and that coherence is required to observe ultrasonic modulation of multiply scattered light. However, the white light source had a broad divergent beam, whereas the laser had a narrow collimated beam. The effect of beam size and collimation has yet to be investigated.

Both scattering and clear objects were imaged using focused ultrasound when they were buried in the center of a background turbid medium (22,26). When the ultrasonic focus was moved from the background turbid medium into the scattering object that had an enhanced absorption coefficient, the ultrasound-modulated optical signal decreased. When the ultrasonic focus was moved from the background turbid medium into the clear medium, the ultrasound-modulated optical signal was comparable with that from the background turbid medium. When the ultrasonic focus was in the clear object, there was little modulation of displacement of scattering particles. If photon–phonon interactions had been insignificant, a much reduced ultrasound-modulated optical signal should have been observed. Therefore, photon–phonon interaction was a significant mechanism. However, scatterer displacement modulation could not be ruled out by this experiment. Further studies are necessary to compare the relative importance of approaches 2 and 3 under various experimental conditions.

MODEL BASED ON ULTRASONIC MODULATION OF SCATTERER DISPLACEMENT

Leutz and Maret reported the observation and theoretical analysis of ultrasonic modulation of multiple-scattering speckles (23). A 5 mm thick glass cuvette filled with scattering medium was illuminated with a laser beam. An ultrasonic wave propagated through the medium perpendicular to the optical axis. The field autocorrelation function of the transmitted light was detected using an electronic autocorrelator by photon counting. A theory was presented to model the scatterer displacement approach (approach 2) in the mod-

ulation mechanisms. Weak scattering approximation was assumed, *i.e.* the scattering mfp of light between successive scatterers along a scattering path was much greater than the wavelength of light, and there was no correlation between the different random paths. The field autocorrelation function was formulated as

$$g_1(t) = \langle E(0)E^*(t)\rangle = \int_{L_t'}^{\infty} p(s)\langle E_s(0)E_s^*(t)\rangle\, ds, \qquad (1)$$

where t is the correlation time, E_s is the electrical field component of the light scattered along a path of length s, E is the overall electrical field component, p(s) is the probability density function of path length s and L_t' is the transport mfp of the turbid medium.

For ultrasonic displacements much less than the wavelength of light,

$$g_1(t) = \int_{L_t'}^{\infty} p(s)\exp\left\{-\frac{2s}{L_t'}\left[\frac{t}{\tau_0} + (k_0A)^2(1 - \cos[\omega_a t])\alpha\right]\right\} ds, \qquad (2)$$

where τ_0 is the single scattering particle relaxation time due to Brownian motion, which is also called characteristic diffusion time (27); k_0 is the wave vector of light, *i.e.* $2\pi/\lambda_0$, where λ_0 is the wavelength of light; A is the amplitude of ultrasonic displacement and ω_a is the angular frequency of ultrasound, *i.e.* $2\pi f_a$, where f_a is the frequency of ultrasound.

$$\alpha = \frac{1}{6} - \frac{\sin(k_aL_t')}{2(k_aL_t')} - \frac{\cos(k_aL_t')}{(k_aL_t')^2} + \frac{\sin(k_aL_t')}{(k_aL_t')^3}, \qquad (3)$$

where k_a is the wave vector of ultrasound, *i.e.* $2\pi/\lambda_a$, where λ_a is the wavelength of ultrasound.

If a plane wave is incident on a slab of thickness L, the transmitted light at a point detector has the field autocorrelation function

$$g_1(t) = \frac{\sqrt{a\{bt + c[1 - \cos(\omega_a t)]\}}}{\sin\sqrt{a\{bt + c[1 - \cos(\omega_a t)]\}}}, \qquad (4)$$

where

$$a = 6(L/L_t')^2, \qquad (5)$$

$$b = 1/\tau_0, \qquad (6)$$

$$c = (k_0A)^2\alpha. \qquad (7)$$

An example of the field autocorrelation function was obtained using Eq. 4 (Fig. 3a). The following typical parameters were used for the computation: L = 5 mm, L_t' = 1 mm, λ_0 = 632.8 nm, τ_0 = 10 ms (27), f_a = 1 MHz, λ_a = 1.5 mm and A = 10 nm. The oscillation was caused by ultrasonic modulation, whereas the decay was caused by Brownian motion.

The intensity spectrum of light may be obtained using Fourier transform of the field autocorrelation function based on the Wiener–Khintchin theorem (Fig. 3b). A strong DC component was truncated in this figure. A fundamental component at the ultrasonic frequency can be clearly seen in the figure, whereas the second harmonic component was much weaker than the fundamental component.

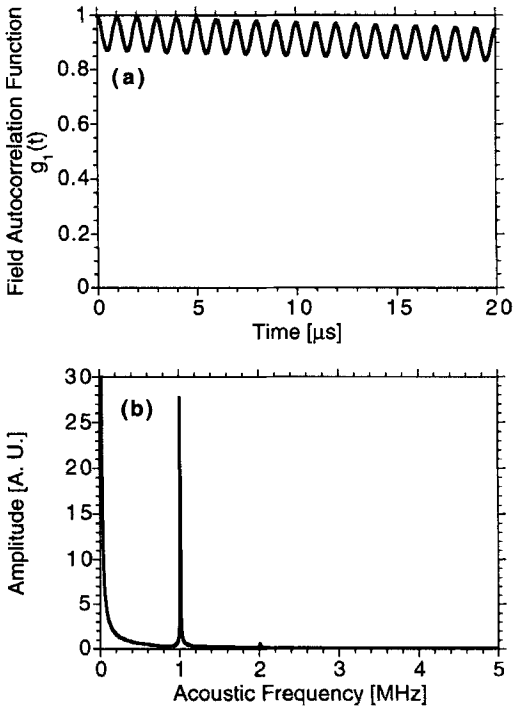

Figure 3. a: A field autocorrelation function of light transmitted through an ultrasound-modulated turbid medium. b: The intensity spectrum of light obtained using the Fourier transform of the field autocorrelation function.

THEORETICAL CONSIDERATION OF SIGNAL DETECTABILITY

For tomographic imaging purposes, a focused ultrasonic wave was used to image objects buried in turbid media (Fig. 1) (21,22). The modulated light carried the information of the optical and mechanical properties near the focal zone, where the modulation off focus was assumed to be less than that at the focus. The ultrasound-modulated optical signal can be separated from the unmodulated light signal by an electronic filter. Scanning the imaging system relative to the turbid medium would generate an image of the medium based on the distribution of optical and mechanical properties.

Detectability of ultrasonic modulation of diffuse light was estimated using diffusion theory for an infinite turbid medium. The following Green's function was used to estimate photon transport from an isotropic point source of unity power (1 W) to a point of observation.

$$G(r) = \frac{\exp(-\mu_{eff}r)}{4\pi Dr}, \qquad (8)$$

where G(r) is the fluence rate at the point of observation that was r away from the light source (W/cm^2), r is the distance between the point of observation and the light source (cm), μ_{eff} is the effective attenuation coefficient (cm^{-1}) and D is the diffusion constant (cm).

The diffusion constant and the effective attenuation coefficient were calculated based on the optical properties of the turbid medium:

Table 1. Results of theoretical calculation of ultrasound-modulated optical power

μ_a (cm^{-1})	μ'_s (cm^{-1})	r_{st} (cm)	r_{fd} (cm)	P_d (W)	N_d (photons*/s)
0.02	10	2.5	2.5	9.6×10^{-11}	4.8×10^{8}
0.02	10	0.5	4.5	2.6×10^{-10}	1.3×10^{9}
0.02	10	5	5	4.9×10^{-13}	2.5×10^{8}
0.1	10	2.5	2.5	8.3×10^{-13}	4.2×10^{6}
0.1	10	0.5	4.5	2.3×10^{-12}	1.2×10^{7}
0.1	10	5	5	3.4×10^{-17}	1.7×10^{2}

*At 1 μm wavelength.

$$D = \frac{1}{3(\mu_a + \mu'_s)} \tag{9}$$

$$\mu_{eff} = \sqrt{\mu_a/D}, \tag{10}$$

where μ_a is the absorption coefficient of the turbid medium (cm^{-1}) and μ'_s is the reduced scattering coefficient of the turbid medium (cm^{-1}).

A collimated laser beam may be modeled using an isotropic point source that was 3D ($=1/(\mu_a + \mu'_s)$) away from the incidence point along the direction of the laser beam. For the optical properties and geometry we considered, the distance 3D was insignificant compared to the distance between the light source and the point of observation. Therefore, the collimated laser beam was replaced with an isotropic point source at the point of incidence for simplicity without losing the validity of the estimation.

Some of the light from the source was transported to the ultrasonic focus, modulated by the ultrasound and then transported to the detector. The modulated signal at the focus was considered a source and re-emitted and part of it reached the detector as estimated by

$$\phi_{ac} = P_s G(r_{sf}) A_m m G(r_{fd}), \tag{11}$$

where ϕ_{ac} is the fluence rate of modulated light at the detector (W/cm^2), P_s is the power of the light source (W), r_{sf} is the distance between the light source and the ultrasonic focus (cm), A_m is the surface area of ultrasound modulation volume (cm^2), m is the modulation depth of light intensity and r_{fd} is the distance between the ultrasonic focus and the detector (cm).

The flux into the detector may be calculated from the fluence rate at the detector as follows.

$$J_+ = \frac{\phi_{ac}}{4} - \frac{D}{2}\frac{\partial \phi_{ac}}{\partial z}\bigg|_{z=r_{fd}} = \frac{\phi_{ac}}{4}[1 + 2D(\mu_{eff} r_{fd} + 1)/r_{fd}], \tag{12}$$

where J_+ is the flux (current density) into the detector in the +z direction (W/cm^2) and z is the axis from the light source to the detector (cm).

The detected power by an ideal detector with a 2π radian acceptance solid angle may be calculated by

$$P_d = J_+ A_d, \tag{13}$$

where P_d is the detected power of modulated light (W) and A_d is the detection area of the detector (cm^2).

Table 1 lists the calculated results for various parameters. The surface area of modulation was assumed to be that of a cylinder 0.2 cm in diameter and 0.2 cm in height. The modulation depth m was assumed to be 10^{-5} based on the experimentally observed modulation depth. The source power P_s of the laser was assumed to be 0.01 W. The detection area of the detector was assumed to be 1 cm^2.

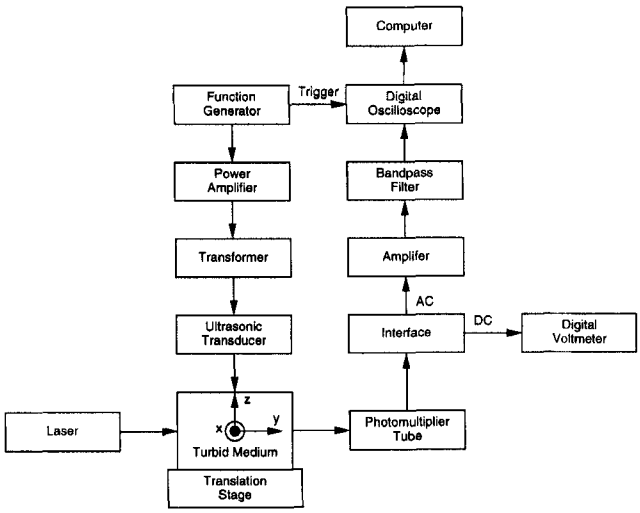

Figure 4. A block diagram of the experimental setup.

The unit W for the detected power P_d may be converted into photons/s (N_d in Table 1) based on the photon energy. For light of 0.5 μm wavelength, 1 J energy contains 2.5×10^{18} photons. For 1 μm wavelength light, 1 J energy contains 5.0×10^{18} photons. If 1 μm wavelength is used, 9.6×10^{-11} W corresponds to 4.8×10^{8} photons/s and 3.4×10^{-17} W corresponds to 170 photons/s.

EXPERIMENTAL SETUP

A block diagram of the experimental setup is shown in Fig. 4. A glass cuvette containing turbid medium was seated on a two-dimensional translation stage. While the cuvette was translated, the rest of the system, including the optical and ultrasonic systems, was fixed.

A He-Ne laser with 10 mW output power and 632.8 nm wavelength delivered a Gaussian beam perpendicular to the front surface of the cuvette. The lower end of the ultrasonic transducer was buried in the liquid turbid medium to allow a good coupling of the ultrasonic wave. If gel turbid media were used, they were covered with liquid turbid media for the coupling purpose. The room lights were turned off to reduce the ambient noise collected by the PMT. An aperture was placed in front of the PMT to control the amount of light entering the PMT.

A function generator produced a sinusoidal wave at a fixed frequency of 1 MHz. This signal drove the ultrasonic transducer after being amplified by a power amplifier and a transformer.

The operating bandwidth of the ultrasonic transducer was centered at 1 MHz. The diameter of the active element of the ultrasonic transducer was 1.9 cm. The focal length of the transducer in water was 3.68 cm. The diameter of the ultrasonic focal spot in water was 0.29 cm. The electric power consumed by the transducer was 210 mW, ~50% of which was converted into ultrasonic power. The peak pres-

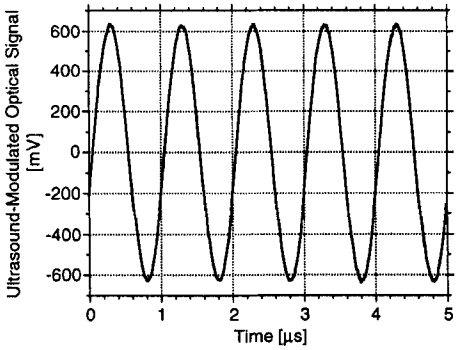

Figure 5. A typical AC electronic signal representing ultrasound-modulated optical (acousto-optical) signal.

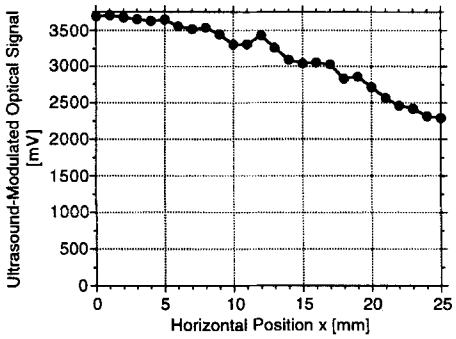

Figure 6. The peak-to-peak AC voltage as a function of the horizontal position of the PMT on the x-axis.

sure at the focus was ~2 bars, which was below the maximum allowed pressure for ultrasonic diagnostics (28).

After light passed through the aperture and reached the PMT, the optical signal was converted into electronic signal. The electronic signal was separated into DC and AC components by an interface circuit. The DC voltage was read by a digital voltmeter, and the AC voltage was amplified and then effectively filtered by a narrow bandpass filter. The filtered signal was collected and averaged over multiple sweeps by a digital oscilloscope, which was triggered by a reference signal from the function generator. Both frequency filtering and signal averaging enhanced the signal-to-noise ratio. The averaged time domain signal was then transferred to a computer for data storage and processing. The peak-to-peak voltage of the AC signal represented the ultrasound-modulated optical signal, whereas the DC signal represented the unmodulated optical signal.

To obtain an image of the turbid medium the cuvette was translated and the AC signal was recorded at each position. Once the signals of all the scanned positions were obtained an image of the turbid medium containing a buried object was constructed.

For convenience, we set up a Cartesian coordinate system to represent the position of the turbid medium. The x-axis was a horizontal axis perpendicular to the optic axis. The y-axis was the optic axis defined by the laser beam. The z-axis was the ultrasonic axis that was defined by the ultrasonic wave.

ULTRASOUND-MODULATED OPTICAL SIGNAL

A typical AC signal representing ultrasound-modulated optical signal is shown in Fig. 5. The optical properties of the 5 cm thick homogeneous gel turbid medium were $\mu_a = 0.1$ cm^{-1} and $\mu_s' = 10$ cm^{-1}. The period of the sinusoidal function was 1 μs, corresponding to the 1 MHz frequency of the ultrasonic wave.

The signal of ultrasonic modulation of transmitted light was carefully tested to rule out the possibility of electronic interference. When the ultrasonic wave was turned off or blocked using an ultrasound-absorbing rubber, the AC signal was reduced to the level of noise, which was the shot noise caused by the transmitted unmodulated light. When the laser light was blocked and the ultrasonic wave was kept on, the AC signal was reduced to a very low level, which was essentially a measurement of the ambient noise. Therefore, the AC signal must have been generated by the interactions between the ultrasonic wave and the laser light.

A typical DC signal was ~50 V while the AC amplitude was ~700 mV. Based on the gains of the AC and DC branches, the ratio between the AC and DC currents at the PMT anode was estimated to be on the order of 10^{-5}–10^{-6}. The modulation was weak because the compressibility of the medium was on the order of 4.6×10^{-5} $bars^{-1}$ and the peak pressure at the ultrasonic focus was ~2 bars. Furthermore, some transmitted light bypassed the ultrasonic field. The incoherent addition of multiple coherence areas on the detector may be another factor causing the low modulation depth.

The theoretical calculation predicted a modulated signal of approximately 8.3×10^{-13} W at the detector for $\mu_a = 0.1$ cm^{-1}, $\mu_s' = 10$ cm^{-1} and 5 cm sample thickness (Table 1). The observed AC voltage under these conditions was ~700 mV. Based on the gains of the PMT and the AC amplifier in the experimental setup, the estimated AC power was on the order of 10^{-13} W. This agreement could have been fortuitous because the theory did not take into account the effects of factors such as heterodyning and speckles. Nevertheless, the raw modulated signal was not very strong and competed with the shot noise. A sensitive detection system was essential to acquire a good S/N.

The peak-to-peak AC voltage was recorded for various PMT positions along the horizontal x-axis (Fig. 6). The optical properties of the 5 cm thick homogeneous liquid turbid medium were $\mu_a = 0.1$ cm^{-1} and $\mu_s' = 6.2$ cm^{-1}. The PMT was first centered to the optic axis (y-axis) and was then translated away from the optic axis with a 1 mm step size. The AC signal was obtained at each PMT position by measuring its peak-to-peak voltage on the oscilloscope. If the ultrasound-modulated optical signal had depended on ballistic light, the signal should have disappeared when the PMT was moved away from the optic axis. Furthermore, ballistic light was not expected to be significant in this dense turbid medium. The gradual decrease of the AC signal indicated that the ultrasound-modulated optical signal originated from the interactions between diffuse light and ultrasound.

An attempt to model the results in Fig. 6 turned out to be difficult. A preliminary simulation using Eq. 11 showed that the primary region of modulation was at the ultrasonic focus when the light source, the ultrasonic focus and the detector were collinear. However, the contribution from off the ultrasonic focus became significant when the system was not

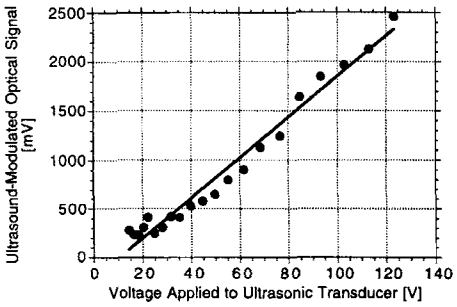

Figure 7. The peak-to-peak AC voltage as a function of the voltage applied to the ultrasonic transducer (solid circles) and a linear fit (solid line).

collinear because the optical path length from the source through the ultrasonic focus to the detector was not the shortest path length between the source and the detector.

The peak-to-peak AC voltage was recorded for various voltage values applied to the ultrasonic transducer (Fig. 7). The optical properties of the 5 cm thick homogeneous liquid turbid medium were $\mu_a = 0.1$ cm^{-1} and $\mu_s' = 10$ cm^{-1}. The AC signal was found to be predominantly linear with the voltage applied to the ultrasonic transducer. The amplitude of the ultrasonic wave was proportional to the voltage applied to the transducer. Therefore, the ultrasound-modulated optical signal was linear with the amplitude of the ultrasonic wave.

The AC signal was also monitored together with the DC signal while the aperture in front of the PMT was varied (22). The AC signal was found to be proportional to the square root of the DC signal and the DC signal was proportional to the area of detection based on simulation. Since the number of speckles collected by the detector was proportional to the area of detection, the AC signal was proportional to the square root of the number of detected speckles, which meant that there was no correlation between the speckle spots.

ULTRASOUND-MODULATED OPTICAL TOMOGRAPHY

A 2D acousto-optical image of an object buried inside a turbid medium was obtained by raster scanning the turbid medium (Fig. 8a). Both the buried object and the background medium were made of gels. The buried object was an approximately 5 mm wide cube. The optical properties of the 5 cm thick background turbid medium were $\mu_a = 0.1$ cm^{-1} and $\mu_s' = 10$ cm^{-1}. The optical properties of the buried object were $\mu_a = 1.1$ cm^{-1} and $\mu_s' = 10$ cm^{-1}. In other words, the absorption coefficient of the buried object was 10 times greater than that of the background medium, while the reduced scattering coefficient of the buried object was the same as that of the background medium. The turbid medium was translated along the x- and z-axes with a 1 mm step size while the detection system was fixed. The ultrasound-modulated optical (AC) signal was recorded at each position. A 2D density plot was then generated after the 2D scanning. For comparison, a 2D DC image of the same object buried inside the same turbid medium was acquired simultaneously while the acousto-optical image was obtained (Fig. 8b). The edge resolution (half maximum) of the AC image of the

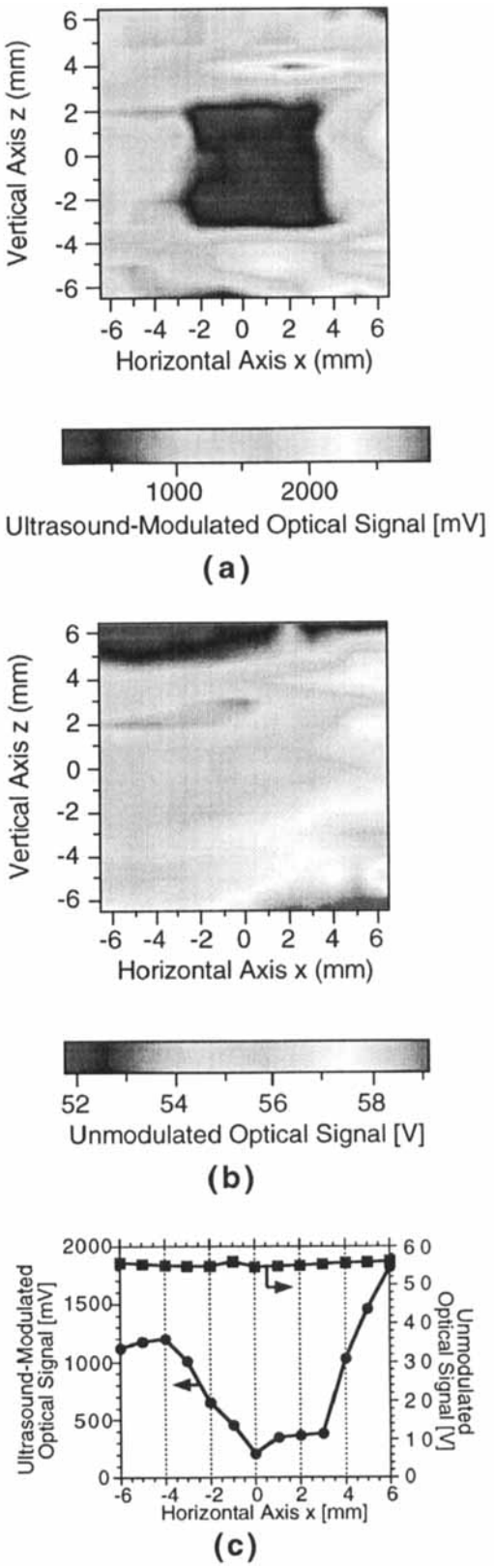

Figure 8. a: A 2D ultrasound-modulated optical (AC) image of an absorbing object buried in a 5 cm thick dense turbid medium. b: A 2D unmodulated optical (DC) image of the same object buried in the same turbid medium. c: A plot of the modulated and unmodulated signals as a function of the horizontal axis x at the origin of the vertical axis z, which were the signals along the horizontal lines crossing the centers of the images in a and b.

buried object was approximately 2 mm, while the buried object was not observable in the DC image (Fig. 8c). This comparison demonstrated how much spatial information the ultrasonic modulation has brought to the diffuse light. The edge resolutions in both the x and z directions were approximately the same. The lateral resolution in the x direction was due to the tight focus of the ultrasound. However, there was no good explanation for the resolution in the z direction because the focus along the ultrasonic axis was less tight.

This imaging technique could potentially be used for breast imaging. The optical properties used in the above turbid medium were comparable to those of real biological tissues. The absorption coefficient may even be reduced if the wavelength of light is appropriately selected.

SUMMARY

In summary, ultrasonic modulation of scattered laser light was used to image absorbing objects buried in tissue-simulating turbid media. Buried objects in 5 cm thick tissue phantoms were imaged with millimeter edge resolution by scanning and detecting alterations of the ultrasound-modulated optical signal. It was experimentally proved that ultrasound-modulated optical tomography depended on diffuse light rather than ballistic light. It was also shown that the ultrasound-modulated optical signal was linearly proportional to the amplitude of the ultrasonic wave. Coherent approaches were likely the dominant mechanism of ultrasonic modulation of light in the experiments on dense turbid media.

The underlying physics of ultrasound-modulated optical tomography is acousto-optics in turbid media. Although acousto-optics in clear media has been well studied (25,29), acousto-optics in turbid media is a new field that may find applications in medicine, underwater detection, atmosphere optics and other fields involving turbid media.

Acknowledgements—We thank X. Zhao and Q. Shen for their experimental assistance. This project was sponsored in part by National Institutes of Health grants R29 CA68562 and R01 CA71980 and The Whitaker Foundation grant.

REFERENCES

1. Jackson, V. P. (1990) The role of US in breast imaging. *Radiology* **77**, 305–311.
2. Jackson, V. P., R. E. Hendrick, S. A. Feig and D. B. Kopans (1993) Imaging of the radiographically dense breast. *Radiology* **88**, 297–301.
3. Fornage, B. D. (1993) Ultrasound of the breast.*Ultrasound Q.* **1**, 1–39.
4. Giger, M. L., C. J. Vyborny and R. A. Schmidt (1994) Computerized characterization of mammographic masses: analysis of spiculation. *Cancer Lett.* **7**, 201–211.
5. Su, B., F. Kappler, B. S. Szwergold and T. R. Brown (1993) Identification of a putative tumor marker in breast and colon cancer. *Cancer Res.* **3**, 1751–1754.
6. Zhou, X. H. and R. Gordon (1989) Detection of early breast cancer: an overview and future prospects. *Crit. Rev. Biomed. Eng.* **7**, 203–255.
7. Alfano, R. R., ed. (1996) *Proceedings of Advances in Optical Imaging and Photon Migration.* Optical Society of America.
8. Chance, B. and R. R. Alfano, eds. (1997) *Optical Tomography and Spectroscopy of Tissue: Theory, Instrumentation, Model, and Human Studies II,* Vol. 2979. Soc. of Photo-Opt. Instrum. Eng.
9. Cheong, W. F., S. A. Prahl and A. J. Welch (1990) A review of the optical properties of biological tissues. *IEEE J. Quantum Electronics* **26**, 2166–2185.
10. Peters, V. G., D. R. Wyman, M. S. Patterson and G. L. Frank (1990) Optical properties of normal and diseased human breast tisseus in the visible and near infrared. *Phys.Med. Biol.* **35**, 1317–1334.
11. Troy, T. L., D. L. Page and E. M. Sevick-Muraca (1996) Optical properties of normal and diseased breast tissues: prognosis for optical mammography. *J. Biomed. Optics* **1**, 342–355.
12. Chance, B., K. Kang, L. He, J. Weng and E. Sevick (1993) Highly sensitive object location in tissue models with linear in-phase and antiphase multielement optical arrays in one and 2 dimensions. *Proc. Natl. Acad. Sci. USA* **90**, 3423–3427.
13. Feng, L., K. M. Yoo and R. R. Alfano (1993) Ultrafast laser-pulse transmission and imaging through biological tissues. *Appl. Optics* **32**, 554–558.
14. Hee, M. R., J. A. Izatt, E. A. Swanson and J. G. Fujimoto (1993) Femtosecond transillumination tomography in thick tissues. *Optics Lett.* **18**, 1107–1109.
15. Wang, L.-H. and S. L. Jacques (1994) Application of probability of n scatterings of light passing through an idealized tissue slab in breast imaging. In *Proceedings of Advances in Optical Imaging and Photon Migration* (Edited by R. R. Alfano), pp. 181–186.
16. Moon, J. A., R. Mahon, M. D. Duncan and J. Reintjes (1993) Resolution limits for imaging throught turbid media with diffuse light. *Optics Lett.* **18**, 1591–1593.
17. Hebden, J. C. and D. T. Delpy (1994) Enhanced time-resolved imaging with a diffusion model of photon transport. *Optics Lett.* **9**, 311–313.
18. Hall, D. J., J. C. Hebden and D. T. Delpy (1995) Time-resolved imaging of a solid breast phantom. *Proc. Soc. Photo-Opt. Instrum. Eng.* **2389**, 182–189.
19. Fishkin, J. B. and E. Gratton (1992) Propagation of photon density waves in strongly scattering media containing an absorbing semi-infinte plate bounded by a straight edge. *J. Opt. Soc. Am. A* **10**, 127–134.
20. Marks, F. A., H. W. Tomlinson and G. W. Brooksby (1993) A comprehensive approach to breast cancer detection using light: photon localization by ultrasound modulation and tissue characterization by spectral discrimination. *Proc. Soc. Photo-Opt. Instrum. Eng.* **1888**, 500–510.
21. Wang, L.-H., S. L. Jacques and X.-M. Zhao (1995) Continuous-wave ultrasonic modulation of scattered laser light to image objects in turbid media. *Optics Lett.* **20**, 629–631.
22. Wang, L.-H. and X.-M. Zhao (1997) Ultrasound-modulated optical tomography of absorbing objects buried in dense tissue-simulating turbid media. *Appl. Optics* **36**, 7277–7282.
23. Leutz, W. and G. Maret (1995) Ultrasonic modulation of multiply scattered light. *Physica B* **204**, 14–19.
24. Kempe, M., M. Larionov, D. Zaslavsky and A. Z. Genack (1997) Acousto-optic tomography with multiply-scattered light. *J. Opt. Soc. Am.* **4**, 1151–1158.
25. Korpel, A. (1988) *Acousto-optics.* Marcel Dekker, New York.
26. Wang, L.-H. and X.-M. Zhao (1997) Ultrasonic modulation of diffuse light in turbid media. *Proc. Soc. Photo-Opt. Instrum. Eng.* **2979**, 24–35.
27. Pine, D. J., D. A. Weitz, P. M. Chaikin and E. Herbolzheimer (1988) Diffusing-wave spectroscopy. *Phys. Rev. Lett.* **60**, 1134–1137.
28. Whittingham, T. A. (1994) The safety of ultrasound. *Imaging* **6**, 33–51.
29. Sapriel, J. (1979) *Acousto-optics.* John Wiley, New York.

Appendix. Nomenclature in tissue optics

Parameters	Definitions	Symbols	Units	Typical
Absorption coefficient	The probability of photon absorption per unit infinitesimal path length	μ_a	cm^{-1}	0.1
Anisotropy	The average of the cosine value of the deflection angle by single scattering	g	—	0.9
Diffusion constant	Linking the gradient of light fluence, $\nabla\phi$, and light current, F (Fick's law), *i.e.* $F = -D\nabla\phi$	D	cm	0.033
Effective attenuation coefficient	The decay constant of light fluence far away from light source; $\mu_{eff} = \sqrt{3\mu_a/D}$	μ_{eff}	cm^{-1}	1.74
Interaction coefficient	The probability of photon interaction per unit infinitesimal path length, where the interaction includes both absorption and scattering. $\mu_t = \mu_a + \mu_s$; sometimes it is also called total attenuation coefficient	μ_t	cm^{-1}	100.1
Mean free path	The mean path length between interactions; $L_t = 1/\mu_t$	L_t	cm	0.0100
Penetration depth	$\delta = 1/\mu_{eff}$; decay constant of the light fluence far from the source	δ	cm	0.575
Reduced scattering coefficient	$\mu_s' = \mu_s(1 - g)$; sometimes it is also called transport scattering coefficient	μ_s'	cm^{-1}	10
Scattering coefficient	The probability of photon scattering per unit infinitesimal path length	μ_s	cm^{-1}	100
Transport interaction coefficient	$\mu_t' = \mu_a + \mu_s'$	μ_t'	cm^{-1}	10.1
Transport mean free path	$L_t' = 1/\mu_t'$	L_t'	cm	0.0990